Atmos. Meas. Tech. Discuss., 4, 1795–1823, 2011
www.atmos-meas-tech-discuss.net/4/1795/2011/
doi:10.5194/amtd-4-1795-2011

Atmospheric Measurement Techniques Discussions

Retrieval of stratospheric aerosol density profiles from SCIAMACHY limb radiance measurements in the O_2 A-band

B. Ovigneur, J. Landgraf, and I. Aben

Netherlands Institute for Space Research (SRON),Utrecht, The Netherlands

Received: 15 February 2011 – Accepted: 17 February 2011 – Published: 15 March 2011

Correspondence to: J. Landgraf (j.landgraf@sron.nl)

Published by Copernicus Publications on behalf of the European Geosciences Union.

Abstract

In this paper we present an approach to retrieve stratospheric aerosol number densities in the altitude range 10–40 km from SCIAMACHY limb radiance measurements in the spectral range of the O_2 A absorption band, near 760 nm. Here, the characteristic light paths differ for the measured light in the O_2 A band and in the spectral continuum next to the absorption band. This difference is used to distinguish the effect of stratospheric aerosol scattering and ground reflection on the limb measurement. The capability to disentangle both effects is illustrated for SCIAMACHY limb observations over the Libyan desert, where the measurements are not affected by tropospheric clouds. Comparison of the SCIAMACHY retrieval and the SAGE II aerosol extinction product between 75 degrees Southern and Northern latitude shows the clear need for prior knowledge of the mean size of the stratospheric aerosol for the SCIAMACHY retrieval. We found best agreement between SCIAMACHY and SAGE II aerosol extinction for the period 2003–2005 for a prior choice of the mean aerosol size radius of 0.2 µm. The overall agreement between both data sets is in the range <50% root mean square difference at 14–30 km with a minimum of 30% at 22 km.

1 Introduction

Fifty years ago, Junge and Manson (1961) reported balloon-borne measurements of the abundance of stratospheric aerosol. Junge and Manson observed a general decrease of the aerosol particle concentration with altitude, but just above the tropopause a layer of larger particles was detected with a vertical extension of several kilometers. This so-called Junge layer consists of supercooled sulfuric acid droplets with different weight percentages of H_2SO_4 in the aerosol and with varying size between 0.1 and 1 µm in diameter.

An important source of the stratospheric aerosol are volcanic eruptions, which can inject a large amount of SO_2 into the stratosphere, where it is photo-oxidized to sulfuric

AMTD
4, 1795–1823, 2011

acid (Hofmann and Rosen, 1983; Oberreck et al., 1983; Deshler et al., 1992, 1993). Hence, volcanic stratospheric aerosols influences directly the heat budget of the atmosphere by absorbing, scattering and emitting radiation depending on their optical properties (Mugnai et al., 1978; McCormick et al., 1995; Solomon, 1999). Close to the tropopause the stratospheric aerosol may affect the formation of cirrus clouds and so it can have an indirect effect on climate and atmospheric photochemistry (Kärcher and Ström, 2003; Penner et al., 2009). Non-volcanic sources of stratospheric aerosol include the transport of OCS from the lower atmosphere to the stratosphere, where it is photochemically transformed into SO_2 (Crutzen, 1976). At present, it is still a outstanding question whether human activities significantly affect the stratospheric aerosol abundance (Hofmann et al., 2009). Next to its climate relevance, stratospheric aerosol interacts with nitrous oxide and chlorine reservoir species (Crutzen, 1970; Fahey et al., 1993) and even small enhancements of the background aerosol level are sufficient to repartition the ozone balance. Thus it is difficult to assess long-term ozone trends without sufficient knowledge on stratospheric aerosol variability.

Several spacecraft-based spectrometers have been launched to monitor stratospheric aerosol through solar occultation, starting with the Stratospheric Aerosol Measurement II (SAM II), which was successfully launched in 1978 (McCormick et al., 1979). Shortly after, in 1979, the Stratospheric Aerosol and Gas Experiment I (SAGE I, McCormick et al., 1982) was launched as the first of a series of three mission dedicated to measure stratospheric aerosols. SAGE I was operational for 34 months. In 1984 and 2001, the SAGE mission got continued with the launch of SAGE II (Mauldin et al., 1985; Bingen et al., 2004a,b) and of SAGE III (Yue, 2000; Chu et al., 2002). After nearly 21 years, the SAGE II instrument was powered off in 2005. The Meteor-3M mission, along with the SAGE III mission, was terminated shortly after, in 2006. Still functional is the Atmospheric Chemistry Experiment (ACE, Bernath et al., 2005) which was launched 2003. Overall this unique series of satellite missions provides a set of more than 40 years of solar occultation measurements of stratospheric aerosols.

AMTD
4, 1795–1823, 2011

Solar occultation measurements allows a straight forward and robust retrieval of aerosol extinction profiles but with the downside of spatially sparse measurements. Alternatively, one can observe stratospheric aerosol from space employing limb viewing geometry, which generally provides a better geographic coverage. The Improved Limb Atmospheric Spectrometer-II (ILAS-II) onboard the Advanced Earth Observing Satellite-II (ADEOS-II) was successfully launched in 2002. However after 10 month ADEOS-II lost its function, and only seven months of data were acquired by the measurements of vertical profiles of aerosol extinction coefficients (Saitoh et al., 2006).Still fully operational are the limb sounding spectrometer OSIRIS (Bourassa et al., 2007) and SCIAMACHY (Bovensmann et al., 1999), both launched in 2001.

SCIAMACHY is an grating spectrometer, whose primary mission objective is to perform global measurements of trace gases in the troposphere and in the stratosphere. It measures the solar radiation, which is backscattered by the atmosphere in nadir, limb and occultation geometry. The relatively high spectral resolution (0.2 nm to 0.5 nm) between 240 nm to 1700 nm, and in selected regions between 2000 nm and 2400 nm, makes it suited for the detection of aerosols (also see Taha et al., 2010). In this paper we present a novel approach in order to retrieve stratospheric aerosol density profiles from SCIAMACHY limb measurements in the O2 A-band. In this spectral range the different atmospheric paths of the measured light allows to disentangle the effect of aerosols and surface reflection on the limb measurement. So, an effective Lambertian surface albedo and a vertical distribution of aerosol density between 10 and 35 km can be retrieved simultaneously from SCIAMACHY limb radiance measurements. This paper is structured as followed: Section 2 analyzes the effect of stratospheric aerosols on SCIAMACHY limb measurements over the Libyan desert between 2003 and 2009. Section 3 describes the retrieval approach and in Sect. 4 the retrieval results are discussed, including a comparison with spatially co-located SAGE II measurements. Finally, the paper is summarized in Sect. 5.

AMTD
4, 1795–1823, 2011

2 Effect of Aerosols on SCIAMACHY limb observations

To demonstrate the sensitivity of limb radiance measurements in the visible and near infrared on aerosol properties, we consider SCIAMACHY limb measurements at 500 nm over the Libyan desert for the period 2004–2009. According to the International Satellite Cloud Climatology Project (ISCCP) cloud information (Rossow and Schiffer, 1999) this region shows very low cloud coverage all the year round. So, the measured light is mainly direct sunlight which is either scattered at the tangent point in the SCIAMACHY viewing direction, or reflected at the Earth surface and subsequently scattered in the instrument's line of sight (see Fig. 1). Here the light can be scattered either by air molecules or stratospheric aerosols. At 500 nm atmospheric absorption by ozone is weak and thus its effect on the measurement is small. The Libyan desert is located around 23 degrees Northern latitudes and so, the solar zenith angle varies between 27 degrees in summer and 70 degrees in winter at the tome of the SCIAMACHY observation. For the limb viewing geometry of SCIAMACHY this causes a variation of the scattering angle of singly scattered light at the tangent point between 55 degrees in winter and 100 degrees in summer. It means that in winter the single scattering geometry is closer to the forward peak of the scattering phase function than in summer. As a result the SCIAMACHY limb radiance varies seasonally as depicted in Fig. 1 for a tangent height of 25 km. To illustrate the different effects of aerosol scattering, Rayleigh scattering, and surface reflection on the measurement, the figure shows different limb radiance simulations for the corresponding measurement geometries. Here we employ the full spherical scalar radiative transfer model of Walter et al. (2006), which includes multiple scattering of light. For an aerosol free atmosphere without surface reflection (red dashed line), the measurements are significantly underestimated by the simulations. Also, the seasonal variation is too weak in the simulation. Enhancing the surface albedo to 0.30 increases the modeled radiance level, but reduces the seasonal variability (green dotted line). The upward radiance at surface level due to Lambertian reflection of the direct solar beam is proportional to the flux $\mu_o F_o \exp(-\tau_o)$ where μ_o

AMTD
4, 1795–1823, 2011

is the cosine of the local solar zenith angle, F_o is the extraterrestrial solar irradiance, and τ_o is the optical thickness along the solar beam from top of the model atmosphere to the surface. At 500 nm, τ_o is very small and so the seasonal dependence of the upwelling intensity at the surface is governed by μ_o. Thus, the upwelling intensity is in antiphase with the single scattering contribution of the measurement, and so enlarging the surface albedo reduces the seasonal variability of the measurement simulation. The blue solid line of Fig. 2 shows a model simulation where we have also added a stratospheric background aerosol to the model atmosphere. Here, the aerosol optical properties are adopted from Loughman et al. (2004) and the corresponding stratospheric aerosol density profile is shown in Fig. 4. Due to the strong forward peak of the aerosol scattering phase function, stratospheric aerosols enhance the seasonal variation of the simulation by increasing the single scattering signal during the winter months.

To compare SCIAMACHY measurements and simulations at different tangent heights, we consider the mean December and June radiances for the period 2004–2009. Figure 3 shows the difference between the measurement and different model simulations as a function of height. Ignoring surface reflection and scattering by stratospheric aerosol results in an underestimation of the measurements by the simulations.

During the winter month the effect is largest around 20–25 km, which hints at the presence of stratospheric aerosols. Surface reflection with an Lambertian albedo of 0.30 enhances the simulation by about the same fraction at all altitudes. This can be explained by the fact that at 500 nm atmospheric absorption and scattering are weak and so, the relative contribution of light that is reflected at the surface is only governed by the scattering properties at the satellite line of sight. The extinction of light between the surface and the scattering point on the line of sight is of little relevance. When we introduce a stratospheric background aerosol in the simulation, we also see an increase of the radiances, which is largest around 20–25 km. Due to that, we expect that adjusting both the surface albedo and the aerosol profile in the lower stratosphere may lead to an improved fit to the data.

AMTD
4, 1795–1823, 2011

Also for the summer month, an albedo of 0.30 enhances the simulated limb radiance signal by nearly the same fraction at all altitudes. However, the aerosol effect is much smaller and causes only a significant change in the limb radiance between 20 and 35 km. Moreover, radiances at tangent heights below 20 km are systematically overestimated for the assumed surface albedo, even when no stratospheric aerosol loading is assumed in the simulation. This is not the case for the winter month, which suggests a seasonal variation of the Lambertian surface albedo.

Figure 2 and 3 indicate that a proper discription of SCIAMACHY limb radiance measurements requires a simultaneous fit of surface albedo and stratospheric aerosol abundances for each individual sequence of limb measurements. For this purpose an appropriate retrieval approach is presented in the following section.

3 Retrieval approach

For the simultaneous retrieval of stratospheric aerosol profiles and surface albedo, we make use of the fact that the measured light mainly follows two characteristics light paths as indicated in Fig. 1. Along the singly scattered light path the amount of measured light is governed by extinction and the scattering probability at the instrument line of sight. Thus, an increase in stratospheric aerosol at tangent height causes an increase in the amount of light traveling this path. The second path includes the reflection of light at the Earth surface and thus increasing surface reflection has the same effect on the limb radiance as increasing the amount of aerosol at the tangent point. For weak atmospheric absorption the relative effect of surface reflection is very similar at different tangent heights (as discussed in the previous section). This makes the simultaneous retrieval of aerosol particle density profiles and surface reflection from limb measurements at one particular wavelength in the longwave visible an ill-posed inversion problem.

To overcome this problem we propose to use limb measurements at different absorption depths of the O_2 A-band including the spectral continuum. Assuming a constant

AMTD
4, 1795–1823, 2011

surface albedo over wavelength, one is able to disentangle the measurement information on albedo and on aerosol concentration due to the different penetration depth of light. For the retrieval the forward model **F** in

$$\boldsymbol{y} = \mathbf{F}(\boldsymbol{x}, \boldsymbol{b}) + \boldsymbol{e}_{\mathrm{y}} \quad (1)$$

has to be inverted, where $\boldsymbol{y}$ is the measurement vector, and $\boldsymbol{x}$ is the state vector, which has the parameters to be retrieved as its components. Vector $\boldsymbol{b}$ contains other model parameters, which have to be chosen a priori, and $\boldsymbol{e}_{\mathrm{y}}$ combines measurement and forward model errors. The measurement vector is defined by a limb scan with tangent heights between 9.5 and 40 km and at three wavelengths, 756, 761, and 772 nm. The shortest and longest wavelength belong to the spectral continuum, whereas the center wavelength is subject to strong oxygen absorption at the lower and middle stratosphere. The height range of the retrieval is determined by two aspects. First, most of stratospheric aerosol is located below 30 km, and so the retrieval captures the most relevant height range. Also, Fig. 5 illustrates that above 44 km the O_2 A band is observed as emission lines in the spectrum. This feature is not taken into account by our forward model and thus limb measurements above 40 km are not used in the retrieval. In this study, we use SCIAMACHY level 1b version 7 data.

In the spectral range of the O_2 A-band multiple scattered light can contribute up to 20% to the total limb radiance. To simulate the limb radiances at the three wavelengths with the SCIAMACHY spectral resolution of 0.5 nm, limb radiances have to be calculated with a line-by-line spherical radiative transfer model on a spectral sampling of at least 0.01 nm. Overall, this makes the forward model simulations computationally demanding. To simplify matters we calculate in each iteration of the retrieval the single scattering contribution on-line, whereas the multiple scattering contribution is approximated by a look-up table as a function of solar geometry, viewing geometry, and surface albedo. The look-up table is precalculated for the background aerosol scenario in Fig. 4. The overall error of the radiance simulation is estimated to be ≤1% for present-day stratospheric aerosol loading.

AMTD
4, 1795–1823, 2011

The state vector $\boldsymbol{x}$ of the retrieval consists of the Lambertian surface albedo and the aerosol density profile, gridded on 3.3 km thick layers between 10 and 40 km. Here, the layer thickness is chosen such that each aerosol element of the state vector can be assigned one-to-one to a limb measurement. Above 40 km, we assume an exponential aerosol height distribution with a relative decrease $\exp(-c\Delta z)$ with $c = 6 \times 10^{-5}\,\mathrm{m}^{-1}$. The model parameter vector $\boldsymbol{b}$ contains the description of the aerosol micro-physical properties. For this study, we assume that the stratospheric aerosol consists of spherical droplets of 25% sulfuric acid and 75% water. The aerosol size is described by a mono-modal log-normal distribution function with a variance of 0.25 µm and with an effective radius of 0.10, 0.15, 0.20, and 0.35 µm for different retrieval scenarios. Using Mie theory, the extinction coefficient, the scattering coefficient, and the scattering phase function are calculated for a refractive index of $r = (1.427, 0.000)$ at 756 nm (d'Almeida et al., 1991). Surface pressure and temperature profiles are taken from the three-hourly forecast of the European Centre for Medium- Range Weather Forecasts (ECMWF2) model, and have been interpolated to the SCIAMACHY overpass time and foot print (cf. http://www.knmi.nl/samenw/tosti/). The absorption cross sections of molecular oxygen are adopted from the Hitran 2008 data base (Rothman et al., 2009).

With the defined state vector $\boldsymbol{x}$ and the model parameter vector $\boldsymbol{b}$, Eq. (1) is inverted by combining a Gauß-Newton iteration with a linear least squares minimization for each iteration step,

$$\hat{\boldsymbol{x}}_{\mathrm{lsq}} = \min_{\mathrm{x}} \|\tilde{\boldsymbol{y}} - \mathbf{K}_{\mathrm{ssc}}\boldsymbol{x}\| \tag{2}$$

with $\tilde{\boldsymbol{y}} = \boldsymbol{y} - \mathbf{F}(\boldsymbol{x}_{\mathrm{o}}, \boldsymbol{b}) + \mathbf{K}_{\mathrm{ssc}}\boldsymbol{x}_{\mathrm{o}}$. Here, the forward model Jacobian is approximated by its single scattering contribution $\mathbf{K}_{\mathrm{ssc}}$ and $\boldsymbol{x}_{\mathrm{o}}$ is the solution of the previous iteration step.

AMTD
4, 1795–1823, 2011

4 Results

Retrieval over Libya

To get a first indication on the performance of the proposed algorithm, we consider the retrieval of stratospheric aerosols over the Libyan desert. In Sect. 2, we mentioned the advantage of these measurements, i.e. the absence of tropospheric clouds, which eases the analysis of the retrieved data. Figure 6 shows the retrieved aerosol density at around 25 km height, assuming a size of 0.35 µm effective radius. The mean aerosol density is about 0.3 particles cm^{-3}, which is a typical stratospheric background concentration at this altitude (e.g. Bingen et al., 2004b). Since the launch of SCIAMACHY, there has been no major volcanic eruption with significant stratospheric sulfur injection and so, the mean retrieved values reflects the present stratospheric abundance. The time series shows a spread of the data around its monthly running value in the order of 0.1 particles cm^{-3}. This is significantly above the retrieval noise level <1% at the altitude range 14–30 km. For the time series in Fig. 6 the SCIAMACHY tangent height varies only by ±100 m and assuming the gradient in the aerosol density profile of Fig. 4 the corresponding fluctuation in the aerosol density is below 0.015 cm^{-3}. This is one order of magnitude below the observed data spread and thus we can rule out variations of the tangent height to explain this feature. To our knowledge stratospheric aerosol at this altitude does not vary on this short time scales and so, we have to address this variation mainly to the effect of measurement biases and forward model errors on the retrieval.

To assess the spectral consistency of the retrieved aerosol properties, we look into the simulations of SCIAMACHY limb radiance measurements at wavelengths in the visible part of the solar spectrum. For the simulation we use the aerosol properties, which are retrieved from SCIAMACHY O_2 A-band measurements. Furthermore, a Lambertian surface albedo is determined for each individual wavelength to account for the spectral variability of surface reflection. Figure 6 shows SCIAMACHY measurements and corresponding radiances simulation at 500 nm. At this wavelength the

AMTD
4, 1795–1823, 2011

limb radiance has significant sensitivity to stratospheric aerosol. In addition, the measurement is only little affected by ozone absorption at the Chappuis absorption band ranging from 440 nm to 1180 nm. So uncertainties on the stratospheric ozone profile are of minor relevance in this context. The lowest two panels of Fig. 6 indicate a small underestimation of the measurement by the simulation of about 5% (±5%). This is slightly larger than the spectral residuals of the aerosol fit in the O_2 A-band (about 3% in the continuum). One possible explanation is the prior choice of aerosol micro-physical properties for the measurement simulations which is not fully suited to describe the correct wavelength dependence. Nevertheless, the retrieved vertical aerosol distribution improves significantly the SCIAMACHY limb measurement simulations in the visible. Keeping in mind that limb radiance measurements at the center of the Chappuis ozone band are used to retrieve ozone in the lower stratosphere (see e.g. von Savigny et al., 2003) the improved forward simulations may be beneficial for these retrievals.

The second panel of Fig. 6 shows the retrieved albedo at 500 nm with a clear seasonal dependence. During summer albedo values around 0.2 are retrieved, whereas during the winter season the retrieved albedo exceeds 0.6. The retrieved albedo is an effective parameter, accounting also for light scattering in the troposphere, which are not properly described in the retrieval. Nevertheless, the seasonal dependence can be addressed to bidirectional reflection at desert surfaces. The third panel of the figure shows a black sky albedo estimate of a desert surface as suggested by Wang et al. (2005) and Briegleb et al. (1986). The black sky albedo is defined as the albedo in the absence of a diffuse downward irradiance at the surface and is a function of solar zenith angle. Both parametrizations show the same seasonal dependence but with a smaller amplitude compared to the retrieved SCIAMACHY albedo. It is important to note that a direct comparison between the black sky albedo and the effective SCIAMACHY albedo is not valid. The SCIAMACHY albedo describes effectively the surface reflection into the upward directed solid angle which influences the limb radiances and which is difficult to estimate. In contrast, the black sky albedo accounts for reflection in the entire upward hemisphere. Nevertheless both albedo result from the same

AMTD
4, 1795–1823, 2011

underlying bidirectional surface reflection, which is the origin of the observed seasonal albedo dependence in the figure.

These first results for SCIAMACHY measurements over the Libyan desert provide confidence in the overall retrieval approach. To get a more quantitative estimate of the retrieval accuracy, a comparison of our retrieval with independent spatially and temporally co-located measurements of stratospheric aerosol is needed.

Comparison with SAGE II

SAGE II provides aerosol extinction profiles at several wavelengths based on solar occultation measurements. For our study we employ SAGE extinction profiles at 525 nm, which are provided by the NASA atmospheric science data center (c.f. http://eosweb.larc.nasa.gov). The SCIAMACHY aerosol particle density profiles are converted to extinction profiles using the micro-physical aerosol properties of the retrieval. To compare both data sets, we consider SAGE and SCIAMACHY aerosol profiles, which are spatially co-located within ±300 km along flight direction and ±115 km across flight direction, and with a measurement time difference of less than 12 h. Figure 7 shows one specific aerosol profile measured by SAGE II and SCIAMACHY over central China. Both profiles show a maximum aerosol extinction of $3 \times 10^{-4}\,\mathrm{km}^{-1}$ between 15 and 18 km. Below 12 km the SCIAMACHY extinction is much larger than the corresponding SAGE extinction. At these altitudes, contamination of the line of sight by thin cirrus clouds may cause the large difference between the two profiles, which does not necessarily indicate an error in one of the retrievals. Above the stratospheric maximum the SAGE profile decays more rapidly and for this case no stratospheric aerosol are reported above 25 km. The SCIAMACHY profile decreases less rapidly towards higher altitudes and non-zero values are found up to 30 km.

For a more extended comparison, we consider about 2000 co-locations between SAGE II and SCIAMACHY measurements for the period January 2003 to June 2005, between 75 degrees Southern and Northern latitude. Figure 8 shows a scattering diagram of co-located SAGE II and SCIAMACHY aerosol extinction coefficients in a

AMTD
4, 1795–1823, 2011

3 km thick layer centered at 25 km. For comparison the SAGE profiles are interpolated linearly to the SCIAMACHY retrieval heights. For a mean radius $\bar{r} = 0.35\,\mu m$, the SCIAMACHY aerosol extinctions exceed significantly the corresponding SAGE values. This is illustrated by a linear regression through the data points where the fitted line is constrained to go through the origin. For $\bar{r} = 0.35\,\mu m$, we obtain a slope of $m = 0.6$ which deviates significantly from the ideal 1-to-1 line. The spread of the data set can be characterized by the mean difference $\delta_m = 1.5 \times 10^{-5}\,km^{-1}$ between the data points and the linear regression.

Figure 9 illustrates the difference between SAGE and SCIAMACHY aerosol extinctions as a function of the scattering angle and latitude of the SCIAMACHY observation. Because of the sun-synchronized orbit of ENVISAT, scattering angle and latitude are correlated. The figure illustrates that differences between SAGE and SCIAMACHY retrievals are smallest at Northern mid-latitudes or for smaller scattering angle. For these cases, the aerosol sensitivity of the measurements is largest and hence forward model errors, e.g. due to a wrong prior estimate of the aerosol size, have a smaller effect on the retrieval than for larger scattering angle. The reduced aerosol sensitivity of the measurement for large scattering angles is also the reason for the little number of successful SCIAMACHY retrievals at the Southern Hemisphere. Figures 8 and 9 also present SCIAMACHY retrieval results for smaller aerosol particles with a mean radius of 0.15 µm. Here, the correlation between SCIAMACHY and SAGE II is clearly improved with a slope of the linear data regression of $m = 1.1$ but with a small effect on the spread with $\delta_m = 1.3 \cdot 10^{-5}\,km^{-1}$. For the smaller aerosols much more retrievals converge for measurements over the Southern hemisphere and the relative difference between both data sets depends less on scattering angle or latitude, respectively. This indicates a better choice of the prior aerosol size and a clear improvement with respect to the previous retrieval.

To illustrate the overall retrieval performance, Fig. 10 shows the slope m and the deviation δ_m as a function of height for different aerosol effective radii of $\bar{r} = 0.10$, 0.15, 0.25, and 0.35 µm. The figure indicates that for $\bar{r} \approx 0.20\,\mu m$ the best correlation can be

AMTD
4, 1795–1823, 2011

achieved. For this radius and above 14 km altitude, a small height dependence of m is present, which may indicate a small increase of the aerosol height at lower altitude. The effect of aerosol size on the deviation δ_m is less pronounced. For $\bar{r} = 0.20\,\mu m$, δ_m varies from 25% of the mean SAGE extinction to < 15% at 22 km. For $\bar{r} = 0.10$ and 0.35 µm, the deviation is somewhat larger. At lower altitudes < 14km, the deviation δ_m increases, which may be caused by the presences of cirrus clouds. Overall the agreement between the SAGE II data product and the presented retrievals is in the order of 30–50% root mean square difference relative to the mean SAGE profile, with a minimum of 30% around 22 km. The investigated data set describes the current stratospheric background aerosol with low particle densities. Bearing this in mind, the achieved agreement between the SAGE II and SCIAMACHY aerosol retrieval not only underlines the suitability of the retrieval concept, but also shows a satisfying quality of the SCIAMACHY retrieval product.

5 Conclusions

In this study, we have presented an approach to retrieve stratospheric aerosol density profiles from SCIAMACHY limb radiance measurements in the spectral range of the O_2 A absorption band around 760 nm. The different paths of the measured light at the spectral continuum with very little atmospheric absorption and at the center of the O_2 absorption band with strong atmospheric absorption allows to disentangle the effect of surface reflection and aerosol scattering on the measurement. Using an iterative least squares minimization, aerosol density profiles are retrieved in the height range 10-40 km. Retrieval simulations for measurements over the Libyan desert with very little cloud contamination showed the capability to determine surface reflection properties and aerosol density profiles. To verify the retrieval quality, about 2000 SCIAMACHY density profiles were compared with SAGE II aerosol extinction retrievals for the period 2003–2005. For this purpose the SCIAMACHY profiles between 75 degrees Southern and Northern latitudes were converted to extinction profiles at 525 nm and so, they could be compared directly with SAGE extinction profiles.

AMTD
4, 1795–1823, 2011

Overall, for background stratospheric aerosol concentrations with low particle densities the SAGE II and SCIAMACHY extinction profiles differ by less than 50% root mean square difference relative to the mean SAGE profile in the altitude range 14–30 km with a best agreement of 30% around 22 km. The SCIAMACHY retrieval performance depends critically on the prior knowledge of the aerosol size. This information cannot be retrieved from the SCIAMACHY O_2 A band measurements, and so an a priori choice had to be made. Here, the best agreement between SAGE and SCIAMACHY retrievals could be achieved for an aerosol effective size radius of $\bar{r} = 0.20\,\mu m$. Due to the different scattering geometry, the SCIAMACHY retrieval performance differs as a function of latitude and aerosol size. At Southern latitudes, and so for larger scattering angles of the limb single scattering geometry, the aerosol sensitivity of the measurement is small. Therefore, the SCIAMACHY retrieval is more sensitive to forward model errors and measurement biases. In turn, only for the smaller aerosol sizes a good convergence performance of the retrieval could be achieved for both the Northern and Southern hemispheres.

The SCIAMACHY aerosol product can be beneficial for other SCIAMACHY limb retrieval products such as stratospheric ozone profile retrieval because of a more accurate forward simulation of the limb radiance measurements. Moreover, the SCIAMACHY aerosol abundances in combination with stratospheric ozone and nitrogen oxide profiles, both retrieved from SCIAMACHY measurements, represents a unique data set of spatially and temporally co-located measurements with a global coverage within 6 days. In the future this data may be useful to improve our knowledge on the long-term chemical evolution of the stratosphere. Nevertheless, further effort is needed for exploiting the full capability of SCIAMACHY limb measurements for stratospheric aerosol retrieval. For example, limb radiance measurements at shorter wavelength may provide useful information on the size of stratospheric aerosol. Furthermore, forward model and measurement errors, e.g. due to the polarization sensitivity of the measurement in the spectral range of strong atmospheric absorption, must be reduced to fully exploit SCIAMACHY limb radiance measurements at all latitudes.

AMTD
4, 1795–1823, 2011

Acknowledgements. This research was funded by the Netherlands Space Office under the project SCIAVISIE. We thank Christian van Savigny, Institute of Environmental Physics (IUP), Bremen, for open and stimulating discussions on the subject of this paper.

References

Bernath, P. F., McElroy, C. T., Abrams, M. C., Boone, C. D., Butler, M., Camy-Peyret, C., Carleer, M., Clerbaux, C., Coheur, P., Colin, R., DeCola, P., DeMazière, M., Drummond, J. R., Dufour, D., Evans, W. F. J., Fast, H., Fussen, D., Gilbert, K., Jennings, D. E., Llewellyn, E. J., Lowe, R. P., Mahieu, E., McConnell, J. C., McHugh, M., McLeod, S. D., Michaud, R., Midwinter, C., Nassar, R., Nichitiu, F., Nowlan, C., Rinsland, C. P., Rochon, Y. J., Rowlands, N., Semeniuk, K., Simon, P., Skelton, R., Sloan, J. J., Soucy, M., Strong, K., Tremblay, P., Turnbull, D., Walker, K. A., Walkty, I., Wardle, D. A., Wehrle, V., Zander, R., and Zou, J.: Atmospheric Chemistry Experiment (ACE): Mission overview, Geophys. Res. Lett., 32, L15S01, doi:10.1029/2005GL022386, 2005. 1797

Bingen, C., Fussen, D., and Vanhellemont, F.: A global climatology of stratospheric aerosol size distribution parameters derived from SAGE II data over the period 1984–2000: 2. Reference data, J. Geophys. Res., 109, D06202, doi:10.1029/2003JD003511, 2004a. 1797

Bingen, C., Fussen, D., and Vanhellemont, F.: A global climatology of stratospheric aerosol size distribution parameters derived from SAGE II data over the period 1984–2000: 1. Methodology and climatological observations, J. Geophys. Res., 109, D06201, doi:10.1029/2003JD003518, 2004b. 1797, 1804

Bourassa, A. E., Degenstein, D. A., Gattinger, R. L., and Llewellyn, E. J.: Stratospheric aerosol retrieval with optical spectrograph and infrared imaging system limb scatter measurements, J. Geophys. Res., 112, D10217, doi:10.1029/2006JD008079, 2007. 1798

Bovensmann, H., Burrows, J. P., Buchwitz, M., Frerick, J., Noël, S., Rozanov, V. V., Chance, K. V., and Goede, A. P. H.: SCIAMACHY: Mission Objectives and Measurement Modes, J. Atmos. Sci., 56, 127–150, 1999. 1798

Briegleb, B. P., Minnis, P., Ramanathan, V., and Harrison, E.: Comparison of Regional Clear-Sky Albedos Inferred from Satellite Observations and Model Computations., J. Appl. Meteorol., 25, 214–226, 1986. 1805, 1819

AMTD
4, 1795–1823, 2011

Chu, W. P., Trepte, C. R., Veiga, R. E., Cisewski, M. S., and Taha, G.: SAGE III measurements, in: Society of Photo-Optical Instrumentation Engineers (SPIE) Conference Series, edited by: W. L. Barnes, vol. 4814 of *Presented at the Society of Photo-Optical Instrumentation Engineers (SPIE) Conference*, 453–460, 2002. 1797

Crutzen, P. J.: The influence of nitrogen oxides on the atmospheric ozone content, Q. J. Roy. Meteor. Soc., 96, 320–325, doi:10.1002/qj.49709640815, 1970. 1797

Crutzen, P. J.: The possible importance of CSO for the sulfate layer of the stratosphere, Geophys. Res. Let., 3, 73–76, 1976. 1797

d'Almeida, G., Koepke, P., and Shettle, E.: Atmospheric Aerosols, Global Climatology and Radiative Characteristics, A. DEEPAK Publishing, Hampton, Virginia USA, 1991. 1803

Deshler, T., Hofmann, D. J., Johnson, B. J., and Rozier, W. R.: Balloonborne measurements of the Pinatubo aerosol-size distribution and volatility at Laramie, Wyoming during the summer of 1991, Geophys. Res. Let., 19, 199–202, 1992. 1797

Deshler, T., Johnson, B. J., and Rozier, W. R.: Balloonborne measurements of Pinatubo aerosol during 1991 and 1992 at 41 deg N – Vertical profiles, size distribution, and volatility, Geophys. Res. Let., 20, 1435–1438, 1993. 1797

Fahey, D. W., Kawa, S. R., Woodbridge, E. L., Tin, P., Wilson, J. C., Jonsson, H. H., Dye, J. E., Baumgardner, D., Borrmann, S., and Toohey, D. W.: In situ measurements constraining the role of sulphate aerosols in mid-latitude ozone depletion, Nature, 363, 509–514, 1993. 1797

Hofmann, D., Barnes, J., O'Neill, M., and Trudeau, M.: Increase in background stratospheric aerosol observed with lidar at Mauna Loa Observatory and Boulder, Colorado, Geophys. Res. Let., 36, L15808, doi:10.1029/2009GL039008, 2009. 1797

Hofmann, D. J. and Rosen, J. M.: Stratospheric sulfuric acid fraction and mass estimate for the 1982 volcanic eruption of El Chichon, Geophys. Res. Let., 10, 313–316, 1983. 1797

Junge, C. E. and Manson, J. E.: Stratospheric Aerosol Studies, J. Geophys. Res., 66, 2163–2182, doi:10.1029/JZ066i007p02163, 1961. 1796

Kärcher, B. and Ström, J.: The roles of dynamical variability and aerosols in cirrus cloud formation, Atmos. Chem. Phys., 3, 823–838, doi:10.5194/acp-3-823-2003, 2003. 1797

Loughman, R. P., Griffioen, E., Oikarinen, L., Postylyakov, O. V., Rozanov, A., Flittner, D. E., and Rault, D. F.: Comparison of radiative transfer models for limb-viewing scattered sunlight measurements, J. Geophys. Res., 109, D06303, doi:10.1029/2003JD003854, 2004. 1800, 1817

Mauldin, L. E., III, Zaun, N. H., McCormick, M. P., Guy, J. H., and Vaughn, W. R.: Stratospheric

AMTD
4, 1795–1823, 2011

Aerosol and Gas Experiment II Instrument: A functional description, Opt. Eng., 24, 307–312, 1985. 1797
McCormick, M. P., Chu, W. P., McMaster, L. R., Hamill, P., Swissler, T. J., and Pepin, T. J.: Satellite studies of the stratospheric aerosol, American Meteorological Society Bulletin, 60, 1038–1046, 1979. 1797
McCormick, M. P., Steele, H. M., Hamill, P., Chu, W. P., and Swissler, T. J.: Polar Stratospheric Cloud Sightings by SAM II., J. Atmos. Sci., 39, 1387–1397, 1982. 1797
McCormick, M. P., Thomason, L. W., and Trepte, C. R.: Atmospheric effects of the Mt Pinatubo eruption, Nature, 373, 399–404, doi:10.1038/373399a0, 1995. 1797
Mugnai, A., Fiocco, G., and Grams, G.: Effects of aerosol optical properties and size distributions on heating rates induced by stratospheric aerosols, Q. J. Roy. Meteor. Soc., 104, 783–796, 1978. 1797
Oberreck, V., Danielsen, E., Snetsinger, K., Ferry, G., Fong, W., and Hayes, D.: Effect of the eruption of El Chichon on stratospehric aerosol size and compostion, Geophys. Res. Let., 10, 1021–1024, 1983. 1797
Penner, J. E., Chen, Y., Wang, M., and Liu, X.: Possible influence of anthropogenic aerosols on cirrus clouds and anthropogenic forcing, Atmos. Chem. Phys., 9, 879–896, doi:10.5194/acp-9-879-2009, 2009. 1797
Rossow, W. and Schiffer, R.: Advances in understanding clouds from ISCCP, Bull. Amer. Meteor. Soc., 80, 2261–2287, 1999. 1799
Rothman, L. S., Gordon, I. E., Barbe, A., Benner, D. C., Bernath, P. F., Birk, M., Boudon, V., Brown, L. R., Campargue, A., Champion, J., Chance, K., Coudert, L. H., Dana, V., Devi, V. M., Fally, S., Flaud, J., Gamache, R. R., Goldman, A., Jacquemart, D., Kleiner, I., Lacome, N., Lafferty, W. J., Mandin, J., Massie, S. T., Mikhailenko, S. N., Miller, C. E., Moazzen-Ahmadi, N., Naumenko, O. V., Nikitin, A. V., Orphal, J., Perevalov, V. I., Perrin, A., Predoi-Cross, A., Rinsland, C. P., Rotger, M., Šimečková, M., Smith, M. A. H., Sung, K., Tashkun, S. A., Tennyson, J., Toth, R. A., Vandaele, A. C., and Vander Auwera, J.: The HITRAN 2008 molecular spectroscopic database, J. Quant. Spectrosc. Radiat. Transfer, 110, 533–572, 2009. 1803
Saitoh, N., Hayashida, S., Sugita, T., Nakajima, H., Yokota, T., Hayashi, M., Shiraishi, K., Kanzawa, H., Ejiri, M. K., Irie, H., Tanaka, T., Terao, Y., Bevilacqua, R. M., Randall, C. E., Thomason, L. W., Taha, G., Kobayashi, H., and Sasano, Y.: Intercomparison of ILAS-II version 1.4 aerosol extinction coefficient at 780 nm with SAGE II, SAGE III, and POAM III, J.

AMTD
4, 1795–1823, 2011

Geophys. Res., 111, D11505, doi:10.1029/2005JD006315, 2006. 1798
Solomon, S.: Stratospheric ozone depletion: A review of concepts and history, Rev. Geophys., 37, 275–316, doi:10.1029/1999RG900008, 1999. 1797
Taha, G., Rault, D. F., Loughman, R. P., Bourassa, A. E., and von Savigny, C.: SCIAMACHY stratospheric aerosol extinction profile retrieval, Atmos. Meas. Tech. Discuss., 3, 5343–5374, doi:10.5194/amtd-3-5343-2010, 2010. 1798
von Savigny, C., Haley, S., Sioris, C., McDade, I., Llewellyn, E., Degenstein, D., Evans, W., Gattinger, R., Griffioen, E., Kyrölä, E., Lloyd, N., McConnell, J., McLinden, C., Mégie, G., Murtagh, D., Solheim, B., and Strong, K.: Stratospheric ozone profiles retrieved from limb scattered sunlight radiance spectra measured by the OSIRIS instrument on the Odin satellite, Geophys. Res. Let., 30, 1755, doi:10.1029/2002GL016401, 2003. 1805
Walter, H. H., Landgraf, J., Spada, F., and Doicu, A.: Linearization of a radiative transfer model in spherical geometry, J. Geophys. Res., 111, D24304, doi:10.1029/2005JD007014, 2006. 1799
Wang, Z., Barlage, M., Zeng, X., Dickinson, R. E., and Schaaf, C. B.: The solar zenith angle dependence of desert albedo, Geophys. Res. Let., L05403, doi:10.1029/2004GL021835, 2005. 1805, 1819
Yue, G. K.: Retrieval of aerosol size distributions and integral properties from simulated extinction measurements at SAGE III wavelengths by the linear minimizing error method, J. Geophys. Res., 105, 14719–14736, 2000. 1797

AMTD
4, 1795–1823, 2011

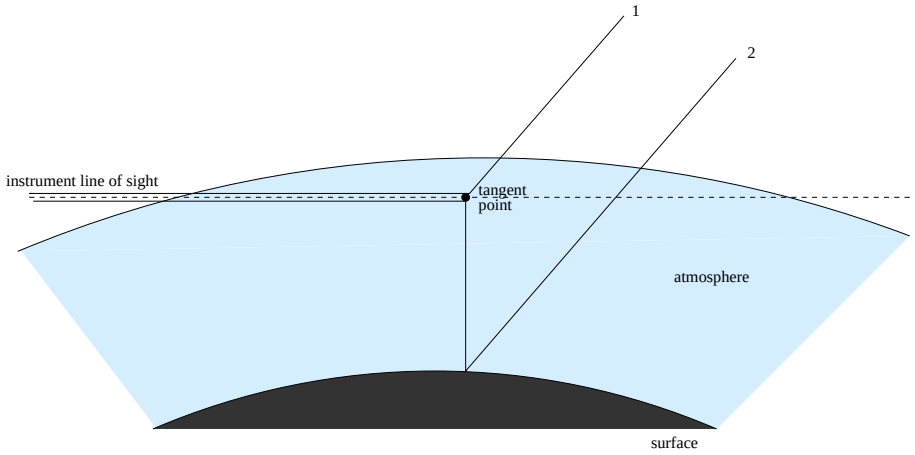

Fig. 1. Two relevant light paths for limb observations in the longwave visible and near infrared. The effect of multiple atmospheric scattering is not presented.

AMTD
4, 1795–1823, 2011

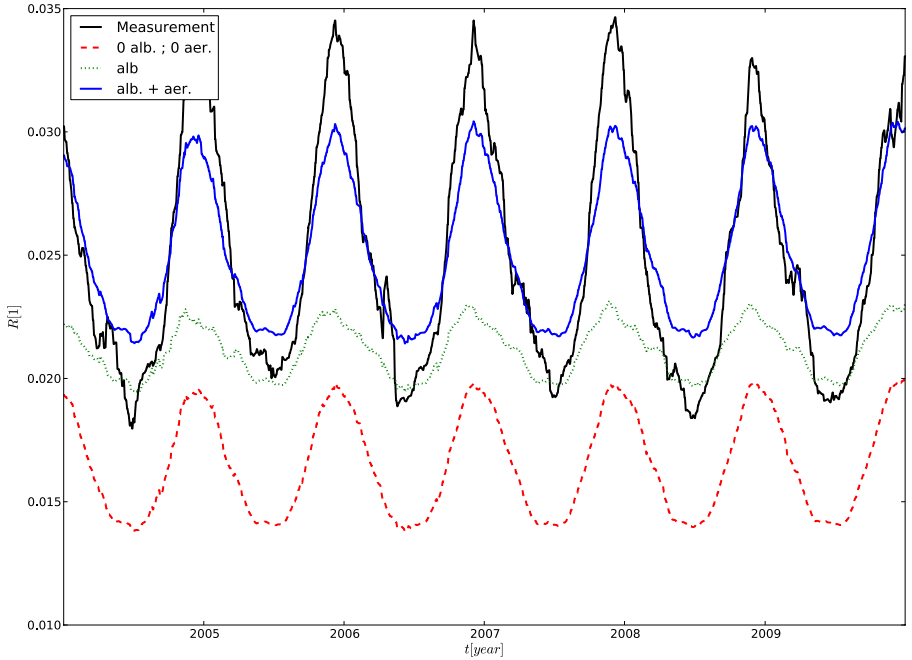

Fig. 2. SCIAMACHY limb radiance measurements at 500 nm over the Libyan desert for tangent height of 25 km as a function of time (black solid line). The Figure shows also three different model simulations using the solar and viewing geometry of the limb observations: for only Rayleigh scattering and no surface reflection (red dashed line), for only Rayleigh scattering and a Lambertian surface albedo of 0.30 (green dotted line), for Rayleigh and background aerosol scattering and a Lambertian surface albedo of 0.30 (blue solid line).

AMTD
4, 1795–1823, 2011

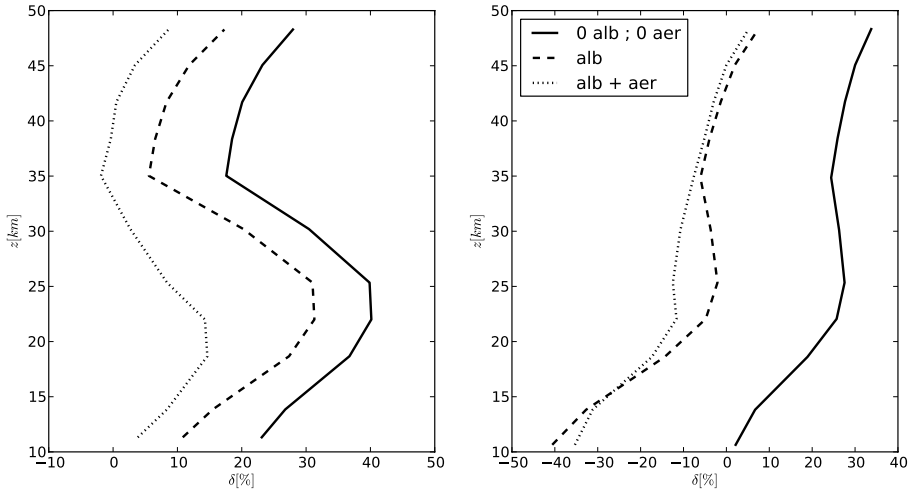

Fig. 3. Differences between monthly mean SCIAMACHY radiances and model simulations (measurement – simulation) as a function of tangent height for December (left panel) and June (right panel) for the period 2004–2009. The model configurations are the same as in Fig. 2.

AMTD
4, 1795–1823, 2011

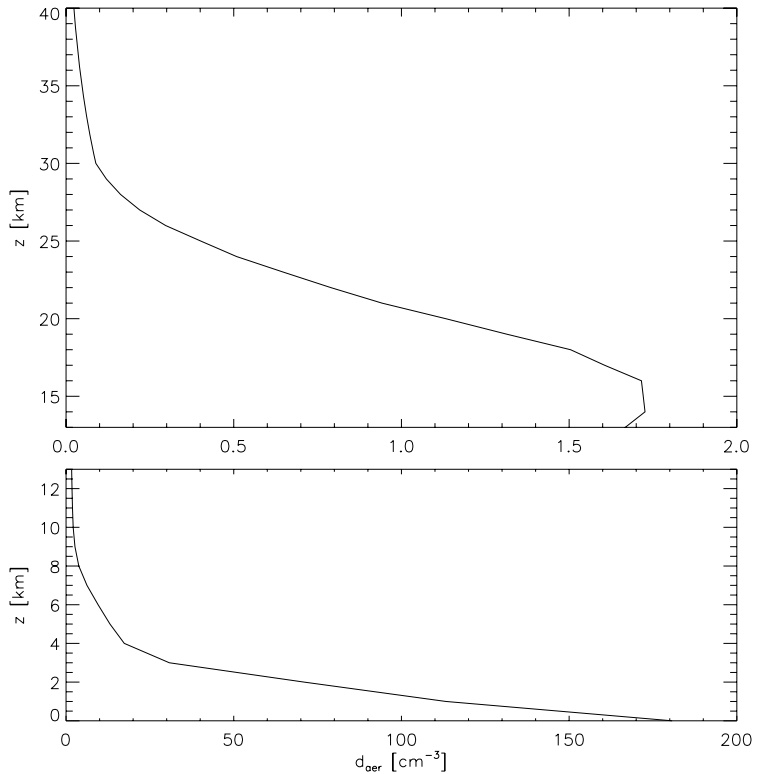

Fig. 4. Profile of aerosol particle density adopted from Loughman et al. (2004). The upper panel shows the stratospheric part of the profile and lower panel the tropospheric part. The profile refers to a background load of stratospheric aerosol.

AMTD
4, 1795–1823, 2011

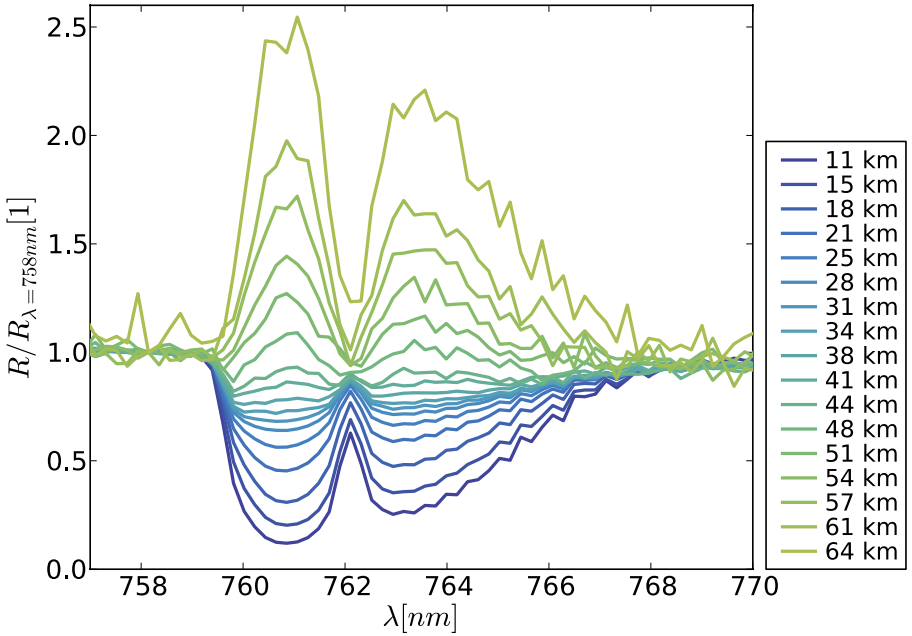

Fig. 5. SCIAMACHY limb radiance measurements in the O_2 A band normalized to the radiance at 758 nm for different tangent heights.

AMTD
4, 1795–1823, 2011

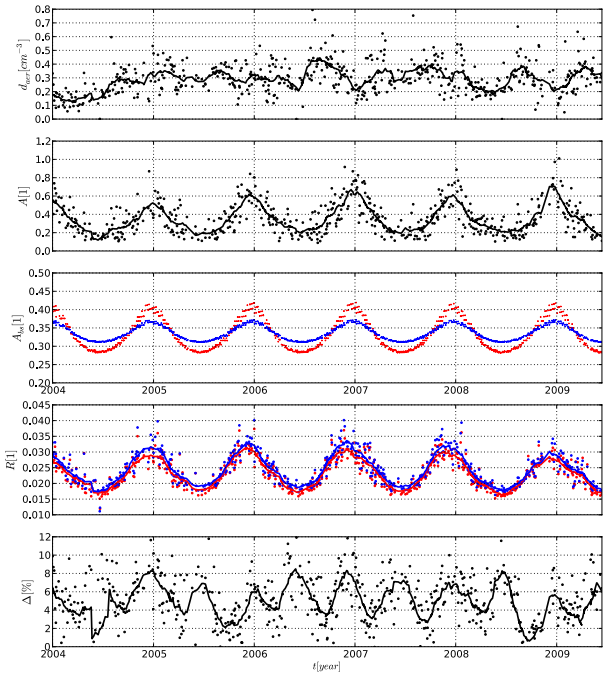

Fig. 6. Stratospheric aerosol density retrieval over the Libyan desert. Dots indicate individual measurements while the solid line represents a one month running mean. (First panel) Aerosol density at 25 km retrieved from SCIAMACHY limb radiance measurements in the O_2 A band. (Second panel) Lambertian surface albedo retrieved at 500 nm. (Third panel) Black sky albedo as a function of time due to its underlying dependence on solar zenith angle as proposed by Briegleb et al. (1986) (red dots) and Wang et al. (2005) (blue dots). (Fourth panel) SCIAMACHY limb radiance measurements at 500 nm at the tangent height closest to 25 km (blue) and forward simulations (red) using the retrieved aerosol profile and the fitted Lambertian surface albedo at 500 nm. (Fifth panel) Relative differences between measurements and simulations.

AMTD
4, 1795–1823, 2011

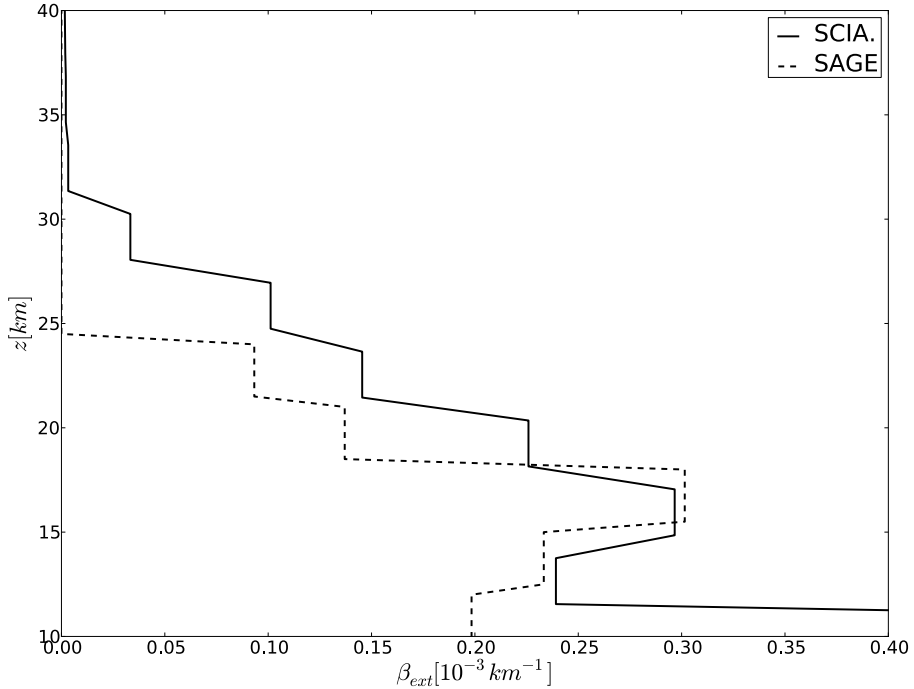

Fig. 7. Spatially and temporally co-located SAGE II and SCIAMACHY aerosol extinction profile at 525 nm above China, 3 January 2003.

AMTD
4, 1795–1823, 2011

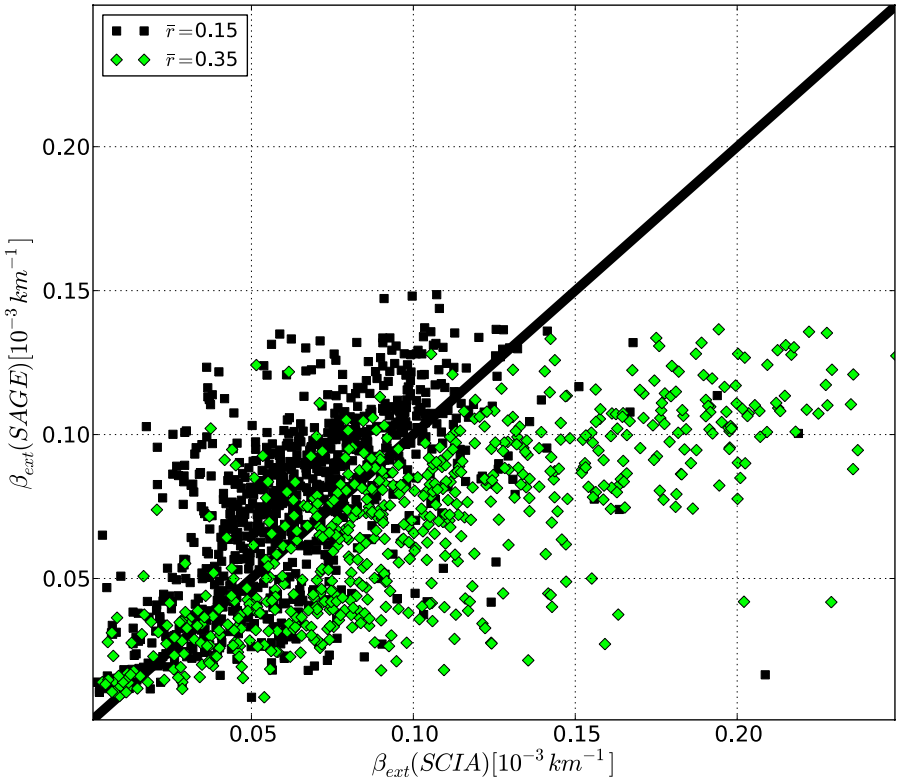

Fig. 8. Scatter diagram of co-located SAGE II and SCIAMACHY aerosol extinction coefficient at 25 km. The black squares indicate SCIAMACHY retrieval with a mean radius $\bar{r} = 0.35\,\mu m$, the green diamonds shows retrieval with $\bar{r} = 0.15\,\mu m$.

AMTD
4, 1795–1823, 2011

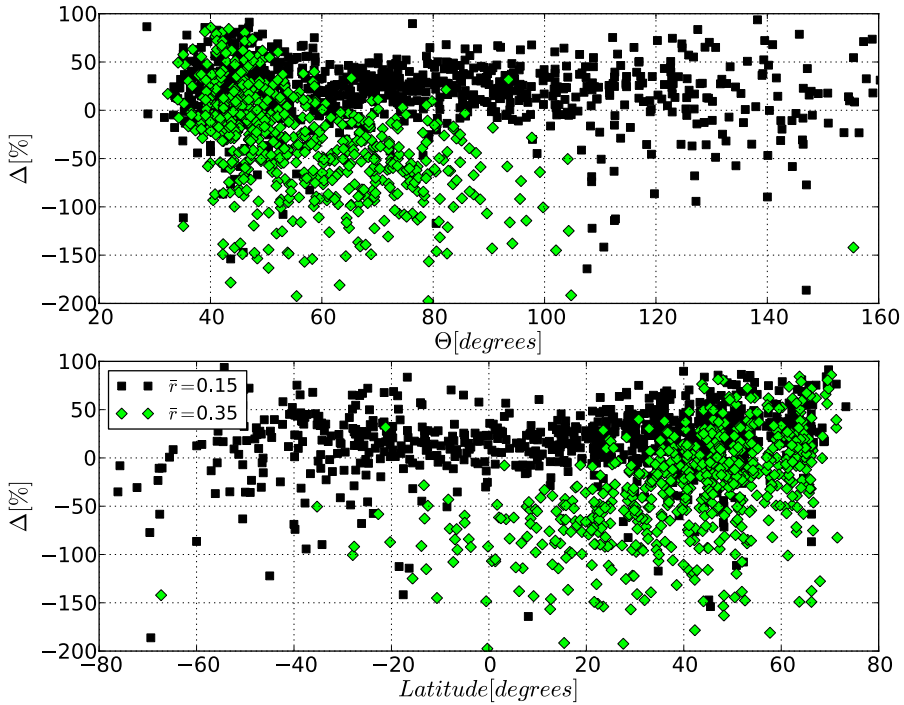

Fig. 9. Relative difference between SAGE and SCIAMACHY aerosol extinction coefficients at 25 km as a function of scattering angle (upper panel) and latitude (lower panel). The black squares indicate SCIAMACHY retrievals with a mean radius $\bar{r} = 0.35\,\mu m$, the green diamonds shows retrievals with $\bar{r} = 0.15\,\mu m$.

AMTD
4, 1795–1823, 2011

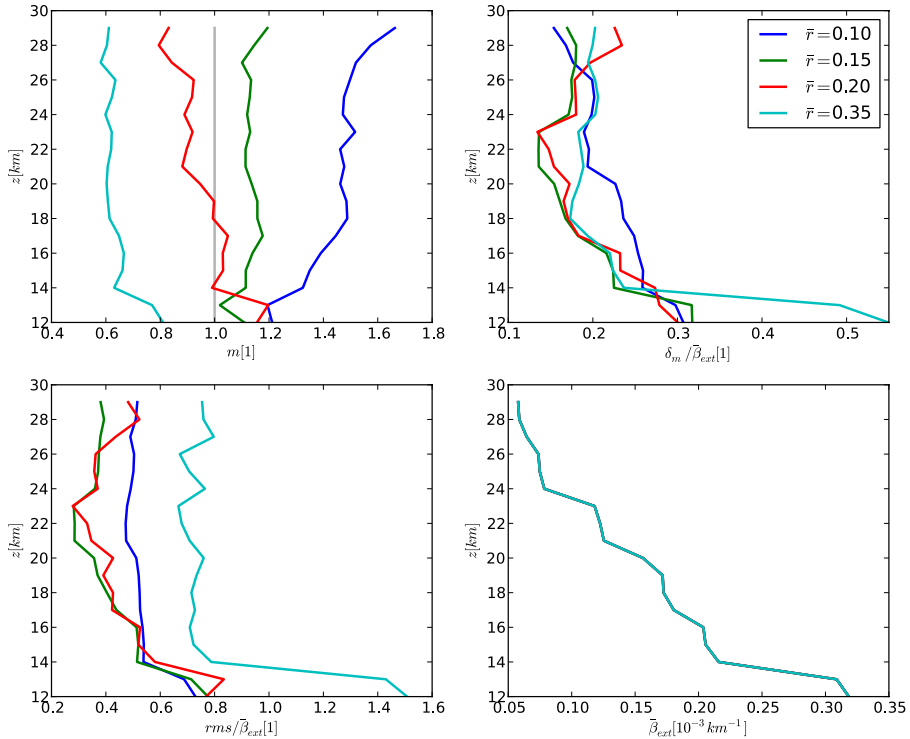

Fig. 10. (Upper left panel) Slope of a linear regression for a scattering diagram as in Fig. 8 as a function of height z. (Upper right panel) Mean deviation from the linear regression δ_m as a function of altitude z, relative to the mean SAGE extinction profile $\bar{\beta}_{ext}$. (Lower left panel) Root mean square difference between SCIAMACHY and SAGE relative to $\bar{\beta}_{ext}$. (Lower right panel) Mean SAGE extinction profile $\bar{\beta}_{ext}$.

AMTD
4, 1795–1823, 2011